Chapter 11

Late evolution of low- and intermediate-mass stars

After the central helium burning phase a central core composed of carbon and oxygen is formed. As discussed before, the further evolution of a star differs greatly between massive stars on the one hand, and low- and intermediate-mass stars on the other hand. The evolution of massive stars, in which the core avoids degeneracy and undergoes further nuclear burning cycles, will be discussed in the next chapter.

In low- and intermediate-mass stars, up to about 8 $M_\odot$, the C-O core becomes degenerate and their late evolution is qualitatively similar. These stars evolve along the so-called *asymptotic giant branch* (AGB) in the H-R diagram. The AGB is a brief but interesting and important phase of evolution, among other things because it is the site of rich nucleosynthesis. AGB stars also suffer from strong mass loss, which eventually removes their envelope and leaves the degenerate C-O core, which after a brief transition stage as the central star of a planetary nebula, becomes a long-lived cooling *white dwarf*.

11.1 The asymptotic giant branch

The AGB phase starts at the exhaustion of helium in the centre. In the examples of the 5 and 1 $M_\odot$ stars discussed in the previous chapter, this occurs at point H in the evolution tracks (Figs. 10.2 and 10.5). The star resumes its climb along the giant branch, which was interrupted by central helium burning, towards higher luminosity. In low-mass stars the AGB lies at similar luminosities but somewhat higher effective temperature than the preceding RGB phase. This is the origin of the name 'asymptotic' giant branch. For stars more massive than about 2.5 $M_\odot$ the AGB lies at higher luminosities than the RGB and the name has no morphological meaning.

One can distinguish two or three phases during the evolution of a star along the AGB. These are highlighted in Fig. 11.1 for our 5 $M_\odot$ example star, but the evolution of lower-mass stars is qualitatively similar.

The early AGB phase

After central He exhaustion the carbon-oxygen core contracts. During a brief transition all layers below the H-burning shell contract (shortly after point H), until He burning shifts to a shell around the CO core. The star now has two active burning shells and a double mirror effect operates: the core contracts, the He-rich layers above expand, and the outer envelope starts contracting. However, due

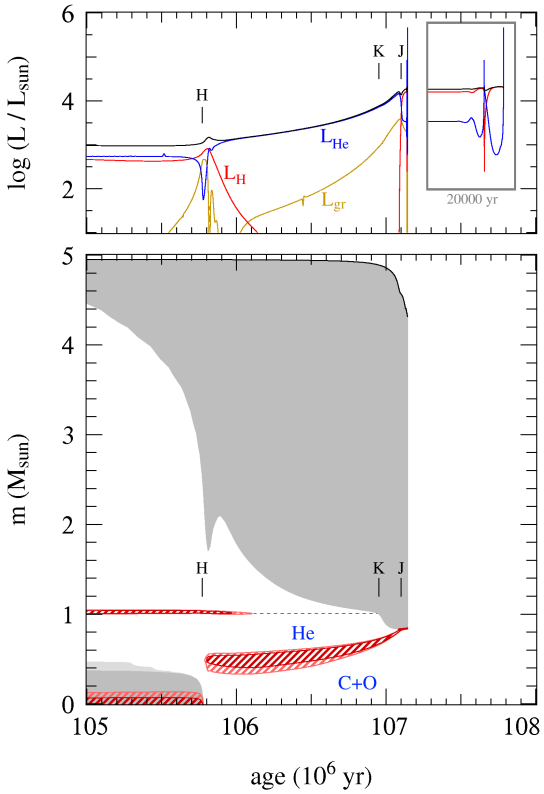

Figure 11.1. Evolution of luminosities (upper panel) and internal structure (lower panel) with time in a 5 $M_\odot$ star (with composition $X = 0.70$, $Z = 0.02$) during the last stages of helium burning and on the AGB. Compare with Fig. 10.3 for the same star. The early AGB starts at point H, when He burning shifts quite suddenly from the centre to a shell around the former convective core. The H-burning shell extinguishes and at point K second dredge-up occurs. The H-burning shell is re-ignited some time later at point J. This is the start of the double shell-burning phase, which soon afterward leads to thermal pulses of the He-burning shell (and break-down of this particular model). The first thermal pulses can be seen in the inset of the upper panel which shows the last 20 000 yr of this model calculation. Strong mass loss is then expected to remove the stellar envelope within $\lesssim 10^6$ yr, leaving the degenerate CO core as a cooling white dwarf.

to expansion of the He-rich zone the temperature in the H-shell decreases and the H-burning shell is extinguished. Thus only one 'mirror' remains and now the entire envelope – He-rich layer plus H-rich outer envelope – starts expanding in response to core contraction. A fairly long-lived phase follows in which the stellar luminosity is provided almost entirely by He-shell burning (phase H-K in Fig. 11.1). This is called the *early AGB* phase.

The He-burning shell gradually adds mass to the growing CO core, which becomes degenerate due to its increasing density. As the envelope expands and cools the convective envelope penetrates deeper until it reaches the composition discontinuity left by the extinct H-shell at point K.

Second dredge-up

In stars of sufficiently high mass, $M \gtrsim 4\,M_\odot$ (depending somewhat on the initial composition and on whether overshooting is included) a convective dredge-up episode can occur, called the *second dredge-up*. At point K in Fig. 11.1 the convective envelope is seen to penetrate down into the helium-rich layers. This is due to a combination of the continuing expansion and cooling of these layers, which increases their opacity, and the growing energy flux produced by the He-burning shell – note that the luminosity has been steadily growing. For lower-mass stars the H-burning shell remains active at a low level, which prevents the convective envelope from penetrating deeper into the star. Consequently, the second dredge-up does not occur in lower-mass stars.

In the material that is dredged up hydrogen has been burned into helium, while ^{12}C and ^{16}O have been almost completely converted into ^{14}N by the CNO-cycle. The amount of He- and N-rich material dredged up is about 0.2 $M_\odot$ in the example shown, and can be as much as 1 $M_\odot$ in the most massive AGB stars. This material is mixed with the outer convective envelope and appears at the surface.

Thus the second dredge-up has a qualitatively similar, but much more dramatic effect that the first dredge-up phase that occurred on the RGB.

An additional important effect of the second dredge-up is the reduction of the mass of the H-exhausted core, thus limiting the mass of the white dwarf that remains. Effectively, the occurrence of second dredge-up thus increases the upper initial mass limit, $M_{\rm up}$, of stars that produce white dwarfs.

The thermally pulsing AGB phase

As the He-burning shell approaches the H-He discontinuity, its luminosity decreases as it runs out of fuel. The layers above then contract somewhat in response, thus heating the extinguished H-burning shell until it is re-ignited. Both shells now provide energy and a phase of *double shell burning* begins. However, the shells do not burn at the same pace: the He-burning shell becomes thermally unstable and undergoes periodic *thermal pulses*, discussed in detail in Sec. 11.1.1. This phase is thus referred to as the *thermally pulsing AGB* (TP-AGB).

The structure of a star during the TP-AGB phase is schematically depicted in Fig. 11.2. The thermally pulsing phase of the AGB has a number of salient properties:

- The periodic thermal pulses alternate with mixing episodes and give rise to a unique *nucleosynthesis* of (among others) ^{12}C, ^{14}N, and elements heavier than iron (Sec. 11.1.2). This process gradually makes the stellar envelope and atmosphere more carbon-rich.
- Similar to the RGB, the stellar properties mainly depend on the size of the degenerate CO core. In particular there is a tight *core mass-luminosity* relation,

$$L = 5.9 \times 10^4 L_\odot \left(\frac{M_{\rm c}}{M_\odot} - 0.52 \right), \tag{11.1}$$

  which is not as steep as the RGB relation (10.2).

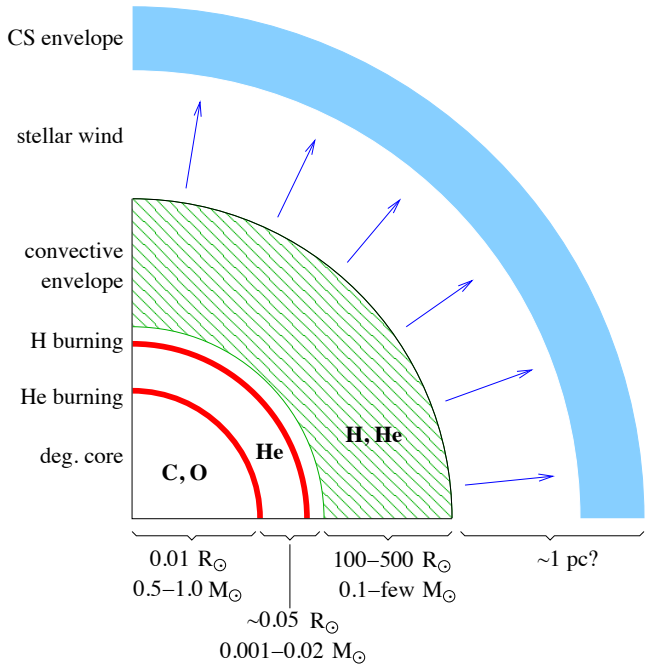

Figure 11.2. Schematic structure of an AGB star during its thermally pulsing phase. The CO core is degenerate and very compact, and is surrounded by two burning shells very close together in mass coordinate. The convective envelope by contrast is very extended and tenuous, having a radius 10^4–10^5 times the size of the core. This loosely bound envelope is gradually eroded by the strong stellar wind, which forms a dusty circumstellar envelope out to several hundreds of stellar radii. The convective envelope, stellar atmosphere and circumstellar envelope have a rich and changing chemical composition driven by nucleosynthesis processes in the burning shells in the deep interior.

- Strong *mass loss* (10^{-7} – 10^{-4} $M_\odot$/yr), probably driven by dynamical (Mira) pulsations combined with radiation pressure on dust particles formed in the cool atmosphere (Sec. 11.1.3), gradually removes the envelope and replenishes the interstellar medium with the synthesized elements.

- The extended stellar atmosphere and circumstellar envelope, formed by the outflow, have a rich molecular and dust chemistry. This is mainly revealed in their infra-red spectra, which have been observed by space telescope missions such as ISO and Spitzer.

11.1.1 Thermal pulses and dredge-up

After the H-burning shell is reignited, the He-burning shell that lies underneath it becomes geometrically thin. Nuclear burning in such a thin shell is thermally unstable, for the reasons discussed in Sect. 7.5.2. This gives rise to periodic *thermal pulses* of the He-burning shell. What happens during a thermal pulse cycle is depicted schematically in Fig. 11.3.

- For most of the time, the He-burning shell is inactive. The H-burning shell adds mass to the He-rich region between the burning shells (the intershell region), which increases the pressure and temperature at the bottom of this region.

- When the mass of the intershell region reaches a critical value, helium is ignited in an unstable manner, giving rise to a thermonuclear runaway called a *helium shell flash*. (Note the difference with the *core* He flash in low-mass red giants, where electron degeneracy causes the thermonuclear runaway.) Values of $L_{\rm He} \approx 10^8\,L_\odot$ are reached during $\sim$ 1 year. The large energy flux drives convection in the whole intershell region (producing an *intershell convection zone*, ICZ).

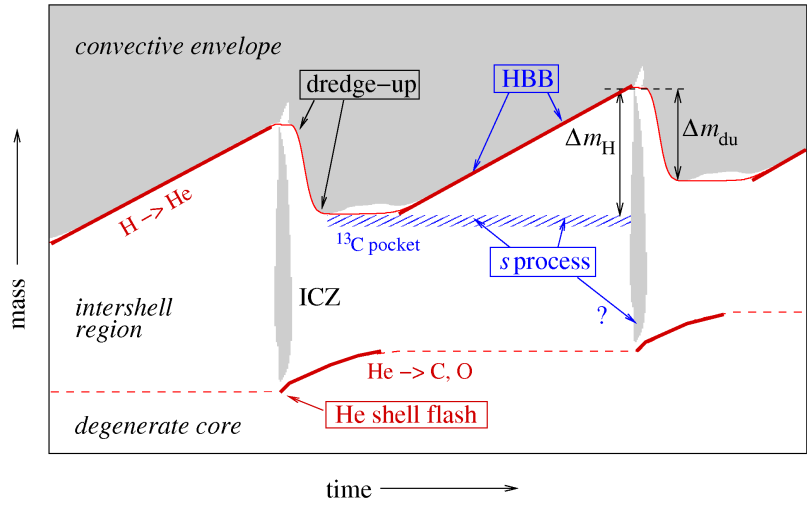

Figure 11.3. Schematic evolution of an AGB star through two thermal-pulse cycles. Convective regions are shown as gray shaded areas, where 'ICZ' stands for the intershell convection zone driven by the He-shell flash. The H-exhausted core mass is shown as a thin red solid line and the He-exhausted core mass as a dashed line. Thick red lines indicate when nuclear burning is active in these shells. Only the region around the two burning shells is shown, comprising $\sim$ 0.01 $M_\odot$. The hatched region indicates a shell or 'pocket' rich in ^{13}C that is formed at the interface of the H-rich envelope and the C-rich intershell region, following a dredge-up episode. Note that the time axis is highly non-linear: the He shell-flash and dredge-up phases (lasting $\sim$ 100 years) are expanded relative to the interpulse phase (10^4 – 10^5 years).

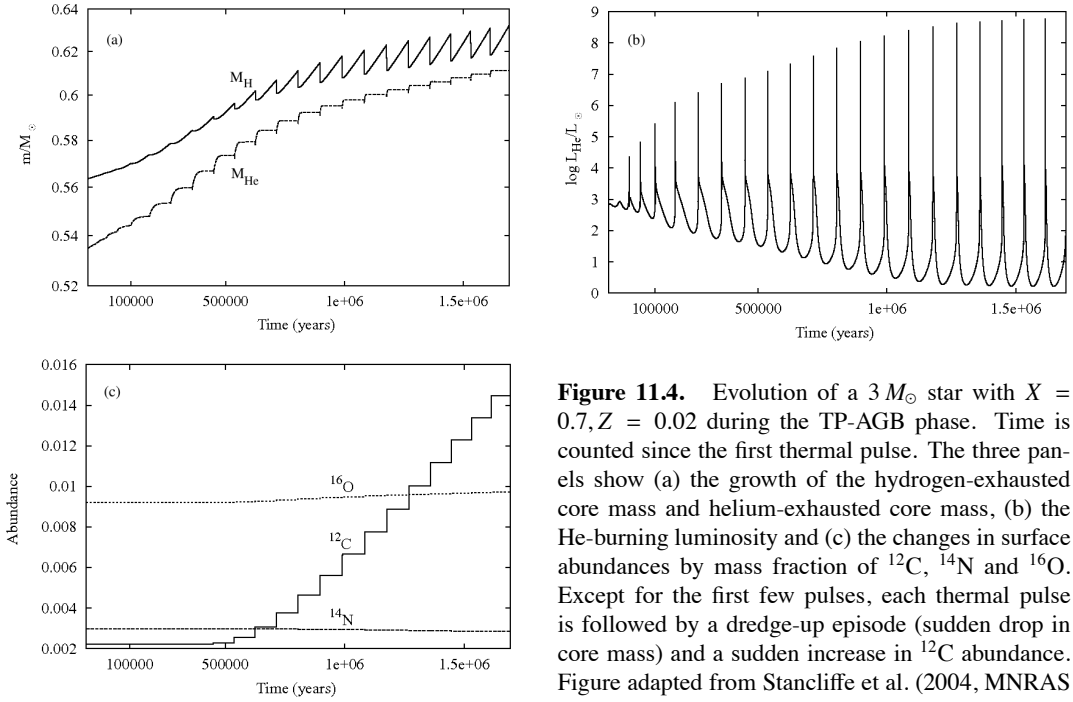

Figure 11.4. Evolution of a $3\,M_\odot$ star with $X = 0.7, Z = 0.02$ during the TP-AGB phase. Time is counted since the first thermal pulse. The three panels show (a) the growth of the hydrogen-exhausted core mass and helium-exhausted core mass, (b) the He-burning luminosity and (c) the changes in surface abundances by mass fraction of ^{12}C, ^{14}N and ^{16}O. Except for the first few pulses, each thermal pulse is followed by a dredge-up episode (sudden drop in core mass) and a sudden increase in ^{12}C abundance. Figure adapted from Stancliffe et al. (2004, MNRAS 352, 984).

This mixes ^{12}C produced by the 3α reaction, as well as other elements produced during He burning, throughout the intershell region.

- The large energy release by the He-shell flash mostly goes into expansion of the intershell region against the gravitational potential. This eventually allows the He-burning shell to expand and cool as well, so that the He-shell flash dies down after several years. A phase of stable He-shell burning follows which lasts up to a few hundred years. As a result of the expansion and cooling of the intershell region after the He-shell flash, the H-burning shell extinguishes.

- Expansion and cooling of the intershell region can also lead to a deeper penetration of the outer convective envelope. In some cases convection can penetrate beyond the now extinct H-burning shell, such that material from the intershell region is mixed into the outer envelope. This phenomenon is called *third dredge-up*. Note that this term is used even for stars that do not experience the second dredge-up, and is used for all subsequent dredge-up events following further thermal pulses. Helium as well as the products of He burning, in particular ^{12}C, can thus appear at the surface.

- Following third dredge-up, the H-burning shell is reignited and the He-burning shell becomes inactive again. A long phase of stable H-shell burning follows in which the mass of the intershell region grows until the next thermal pulse occurs. The duration of this *interpulse period* depends on the core mass, lasting between 50,000 yrs (for low-mass AGB stars with CO cores of $\sim 0.5\,M_\odot$) to < 1000 yrs for the most massive AGB stars.

This thermal pulse cycle can repeat many times, as shown for a $3\,M_\odot$ AGB star in Fig. 11.4. The pulse amplitude (the maximum helium-burning luminosity) increases with each pulse, which facilitates dredge-up after several thermal pulses. In the example shown, third dredge-up first occurs after the 7th thermal pulse ($\sim 5 \times 10^5$ yr after the start of the TP-AGB phase) and then follows after

every subsequent pulse. The efficiency of dredge-up is often measured by a parameter λ, which is defined as the ratio of the mass dredged up into the envelope over the mass by which the H-exhausted core has grown during the preceding interpulse period (see Fig. 11.3),

$$\lambda = \frac{\Delta M_{\rm du}}{\Delta M_{\rm H}}. \tag{11.2}$$

Third dredge-up has two important consequences. First, unlike the first and second dredge-up which only mix up H-burning products, the third dredge-up bring products of *helium burning* to the surface. This leads to important nucleosynthesis (see Sec. 11.1.2). Second, third dredge-up limits the growth of the CO core mass. Efficient dredge-up with $\lambda \approx 1$ means that in the long run, the core mass does not increase.

11.1.2 Nucleosynthesis and abundance changes on the AGB

The main effect of thermal pulses and third dredge-up operating in AGB stars is the appearance of helium-burning products at the surface, in particular a large production of carbon. In the $3\,M_\odot$ model shown in Fig. 11.4, the surface ^{12}C abundance increases after every dredge-up episode and thus gradually increases, until it exceeds the ^{16}O abundance after 1.3×10^6 yr.

At the low temperatures in the stellar atmosphere, most of the C and O atoms are bound into CO molecules, such that the spectral features of AGB stars strongly depend on the C/O number ratio. If n(C)/n(O) < 1 (simply written as 'C/O < 1'), then the remaining O atoms form *oxygen-rich* molecules and dust particles, such as TiO, H_2O and silicate grains. The spectra of such O-rich AGB stars are classified as type M or S. As a result of repeated dredge-ups, at some point the C/O ratio can exceed unity. If C/O > 1 then all O is locked into CO molecules and the remaining C forms *carbon-rich* molecules and dust grains, e.g. C_2, CN and carbonaceous grains like graphite. Such more evolved AGB stars are classified as *carbon stars* with spectral type C.

Besides carbon, the surface abundances of many other elements and isotopes change during the TP-AGB phase. The direct evidence for active nucleosynthesis in AGB stars was the detection in 1953 of technetium, an element with only radioactive isotopes of which the longest-lived one (^{99}Tc) decays on a timescale of 2×10^5 yrs. AGB stars are nowadays considered to be major producers in the Universe of carbon, nitrogen and of elements heavier than iron by the *s-process*. They also make an important contribution to the production of ^{19}F, ^{25}Mg, ^{26}Mg and other isotopes.

Production of heavy elements: the s-process

Spectroscopic observations show that many AGB stars are enriched in elements heavier than iron, such as Zr, Y, Sr, Tc, Ba, La and Pb. These elements are produced via slow neutron capture reactions on Fe nuclei, the so-called *s-process*. In this context 'slow' means that the time between successive neutron captures is long compared to the β-decay timescale of unstable, neutron-rich isotopes.

The synthesis of s-process elements requires a source of free neutrons, which can be produced in the He-rich intershell region by either of two He-burning reactions: ^{13}C$(\alpha, \mathrm{n})^{16}$O and ^{22}Ne$(\alpha, \mathrm{n})^{25}$Mg. The latter reaction can take place during the He-shell flash if the temperature exceeds 3.5×10^8 K, which is only reached in rather massive AGB stars. The ^{22}Ne required for this reaction is abundant in the intershell region, because the ^{14}N that is left by the CNO-cycle is all converted into ^{22}Ne by He-burning: ^{14}N$(\alpha,\gamma)^{18}$F$(\beta^+)^{18}$O$(\alpha,\gamma)^{22}$Ne.

The main neutron source in low-mass stars (up to $3\,M_\odot$) is probably the ^{13}C$(\alpha, \mathrm{n})^{16}$O reaction. The current idea is that a thin shell or 'pocket' of ^{13}C is formed (shown as a hatched region in Fig. 11.3) by partial mixing of protons and ^{12}C at the interface between the H-rich envelope and the C-rich intershell region, which produces ^{13}C by the first step of the CN-cycle. The ^{13}C subsequently reacts

with helium when the temperature reaches 10^8 K, releasing the required neutrons. The s-enriched pocket is ingested into the ICZ during the next pulse, and mixed throughout the intershell region, together with carbon produced by He burning. The carbon and s-process material from the intershell region is subsequently mixed to the surface in the next dredge-up phase (see Fig. 11.3).

Hot bottom burning

In stars with $M \gtrsim 4{-}5\,M_\odot$, the temperature at the base of the convective envelope during the interpulse period becomes so high ($T_{\rm BCE} \gtrsim 3 \times 10^7$ K) that H-burning reactions take place. The CNO cycle then operates on material in the convective envelope, a process known as *hot bottom burning*. Its main effects are: (1) an increase in the surface luminosity, which breaks the core mass-luminosity relation; (2) the conversion of dredged-up ^{12}C into ^{14}N, besides many other changes in the surface composition. Hot bottom burning thus prevents massive AGB stars from becoming carbon stars, and turns such stars into efficient producers of *nitrogen*. Other nuclei produced during hot bottom burning are ^{7}Li, ^{23}Na, and ^{25,26}Mg.

11.1.3 Mass loss and termination of the AGB phase

Once a star enters the TP-AGB phase it can experience a large number of thermal pulses. The number of thermal pulses and the duration of the TP-AGB phase is limited by (1) the decreasing mass of the H-rich envelope and (2) the growing mass of the degenerate CO core. If the CO core mass is able to grow close to the *Chandrasekhar mass*, $M_{\rm Ch} \approx 1.46\,M_\odot$, carbon will be ignited in the centre in a so-called 'carbon flash' that has the power to disrupt the whole star (see Chapter 13). However, white dwarfs are observed in rather young open clusters that still contain massive main-sequence stars. This tells us that the carbon flash probably never happens in AGB stars, even when the total mass is 8 $M_\odot$, much larger than $M_{\rm Ch}$. The reason is that *mass loss* becomes so strong on the AGB that the entire H-rich envelope can be removed before the core has had time to grow significantly. The lifetime of the TP-AGB phase, $1 - 2 \times 10^6$ yr, is essentially determined by the mass-loss rate.

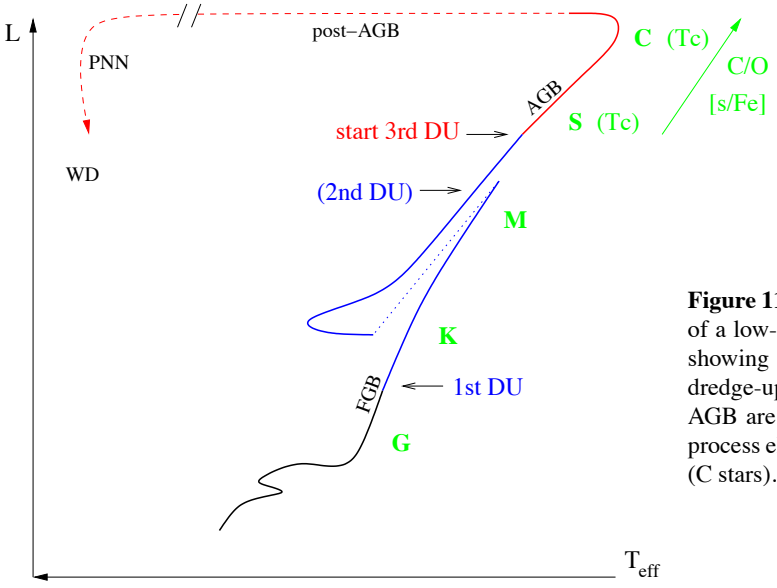

Figure 11.5. Schematic evolution track of a low-mass star in the H-R diagram, showing the occurrence of the various dredge-up episodes. Stars on the upper AGB are observed to be enriched in s-process elements (S stars) and in carbon (C stars).

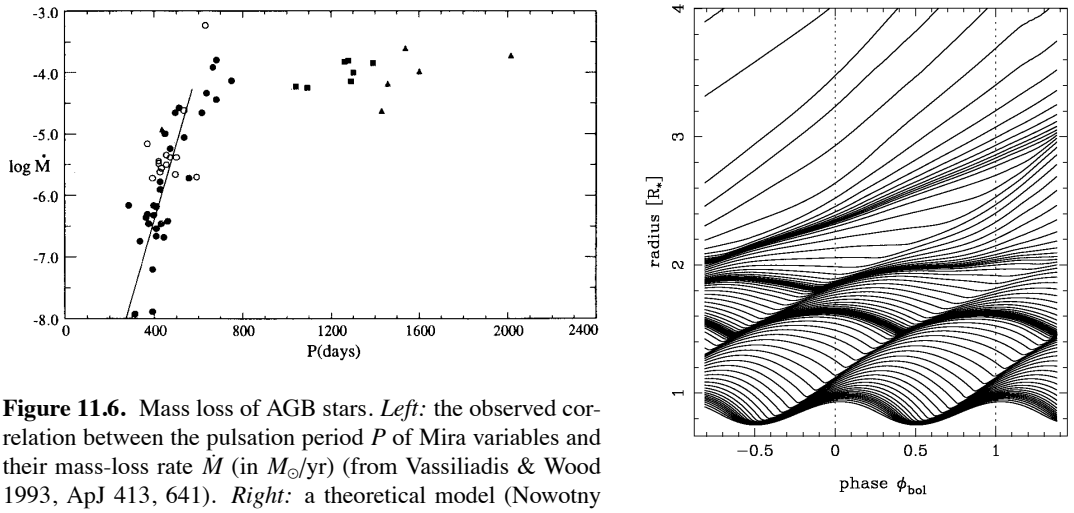

Figure 11.6. Mass loss of AGB stars. *Left:* the observed correlation between the pulsation period P of Mira variables and their mass-loss rate $\dot{M}$ (in $M_\odot$/yr) (from Vassiliadis & Wood 1993, ApJ 413, 641). *Right:* a theoretical model (Nowotny et al. 2005, A&A 437, 273) showing streamlines in the outer atmosphere of an AGB star undergoing radial pulsations. At $r \gtrsim 2\,R_*$ dust particles form in the dense shocked regions and radiation pressure on the dust then pushes the mass out.

AGB mass loss

That AGB stars have strong stellar winds is clear from their spectral energy distributions, which show a large excess at infrared wavelengths. Many AGB stars (known as OH/IR stars) are even completely enshrouded in a dusty circumstellar envelope and are invisible at optical wavelengths. The mechanisms driving such strong mass loss are not yet completely understood, but a combination of dynamical *pulsations* and *radiation pressure* on dust particles formed in the atmosphere probably plays an essential role. Stars located on the AGB in the H-R diagram are found to undergo strong radial pulsations, they are known as *Mira* variables (see Fig. 10.11). An observational correlation exists between the pulsation period and the mass-loss rate, shown in Fig. 11.6a. As a star evolves towards larger radii along the AGB, the pulsation period increases and so does the mass-loss rate, from $\sim 10^{-8}\,M_\odot$/yr to $\sim 10^{-4}\,M_\odot$/yr for pulsation periods in excess of about 600 days.

The basic physical picture is illustrated in Fig. 11.6b. The pulsations induce shock waves in the stellar atmosphere, which brings gas out to larger radii and thus increases the gas density in the outer atmosphere. At about $1.5 - 2$ stellar radii, the temperature is low enough (~ 1500 K) that dust particles can condense. The dust particles are very opaque and, once they have formed, can easily be accelerated by the radiation pressure that results from the high stellar luminosity. In the absence of pulsations, the gas density at such a distance from the star would be too low to form dust. Even though the gas in the atmosphere is mostly in molecular form (H_2, CO, etc.) and the dust fraction is only about 1%, the molecular gas is dragged along by the accelerated dust particles resulting in a large-scale outflow.

Observationally, the mass-loss rate levels off at a maximum value of $\sim 10^{-4}\,M_\odot$/yr (this is the value inferred for dust-enshrouded OH/IR stars, the stars with the largest pulsation periods in Fig. 11.6). This phase of very strong mass loss is sometimes called a 'superwind'. Once an AGB star enters this superwind phase, the H-rich envelope is rapidly removed. This marks the end of the AGB phase. The high mass-loss rate during the superwind phase therefore determines both the maximum luminosity that a star can reach on the AGB, and its final mass, i.e. the mass of the white-dwarf remnant (Fig. 11.7).

Post-AGB evolution

When the mass of the H-rich envelope becomes very small, $10^{-2} - 10^{-3}\,M_\odot$ depending on the core mass, the envelope shrinks and the star leaves the AGB. The resulting decrease in stellar radius occurs at almost constant luminosity, because the H-burning shell is still fully active and the star keeps following the core mass-luminosity relation. The star thus follows a horizontal track in the H-R diagram towards higher effective temperatures. This is the *post-AGB* phase of evolution. Note that the star remains in complete equilibrium during this phase: the evolution towards higher $T_{\rm eff}$ is caused by the decreasing mass of the envelope, which is eroded at the bottom by H-shell burning and at the top by continuing mass loss. The typical timescale for this phase is $\sim 10^4$ yrs.

As the star gets hotter and $T_{\rm eff}$ exceeds 30,000 K, two effects start happening: (1) the star develops a weak but fast wind, driven by radiation pressure in UV absorption lines (similar to the winds of massive OB-type stars, see Sec. 12.1); and (2) the strong UV flux destroys the dust grains in the circumstellar envelope, dissociates the molecules and finally ionizes the gas. Part of the circumstellar envelope thus becomes ionized (an HII region) and starts radiating in recombination lines, appearing as a *planetary nebula*. Current ideas about the formation of planetary nebulae are that they result from the interaction between the slow AGB wind and the fast wind from the central star, which forms a compressed optically thin shell from which the radiation is emitted.

When the envelope mass has decreased to $10^{-5}\,M_\odot$, the H-burning shell is finally extinguished. This happens when $T_{\rm eff} \approx 10^5$ K and from this point the luminosity starts decreasing. The remnant now cools as a white dwarf. In some cases the star can still experience a final thermal pulse during its post-AGB phase (a *late thermal pulse*), or even during the initial phase of white dwarf cooling (a

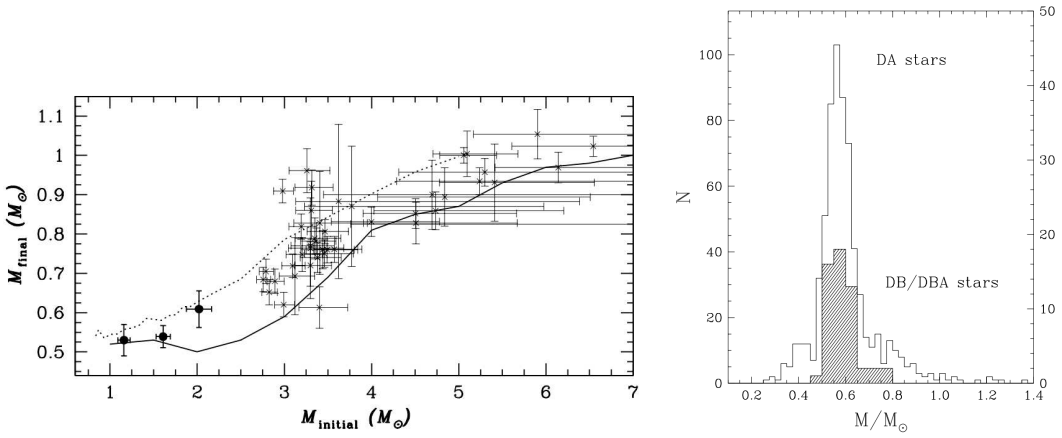

Figure 11.7. *Left:* Relation between between the initial and final mass of low- and intermediate-mass stars, from Kalirai et al. (2008, ApJ 676, 594). The data points represent white dwarfs observed in open clusters, for which the mass has been determined from their spectra. The age of the cluster $t_{\rm cl}$ and the cooling time of the white dwarf $t_{\rm wd}$ have been used to estimate the initial mass, because $t_{\rm cl} - t_{\rm wd}$ corresponds to the lifetime of the progenitor star. The solid line shows model predictions for the core mass of a star at the start of the TP-AGB phase (from Marigo 2001, A&A 370, 194) for solar metallicity. The dotted line shows the final mass of these models, which is reasonably consistent with the data points. The growth of the core mass on the AGB is severely limited by dredge-up and strong mass loss.

Right: Observed mass distribution of white dwarfs, for a large sample of DA white dwarfs and a smaller sample of DB white dwarfs (from Bergeron et al. 2007). There is a sharp peak between 0.55 and 0.6 $M_\odot$, as can be expected from the initial-final mass relation because most white dwarfs come from low-mass stars with $M < 2\,M_\odot$.

very late thermal pulse). This can temporarily bring the star back to the AGB (sometimes referred to as the 'born-again AGB' scenario).

11.2 White dwarfs

All stars with initial masses up to about $8\,M_\odot$ develop electron-degenerate cores and lose their envelopes during the AGB phase, and thus end their lives as white dwarfs. Nuclear fusion no longer provides energy and white dwarfs shine by radiating the thermal energy stored in their interiors, cooling at almost constant radius and decreasing luminosities. The faintest white dwarfs detected have $L \approx 10^{-4.5}\,L_\odot$. Observed WD masses are mostly in a narrow range around $0.6\,M_\odot$, see Fig. 11.7b, which corresponds to the CO core mass of low-mass ($\lesssim 2\,M_\odot$) AGB progenitors. This sharply peaked mass distribution, along with the observationally induced initial-to-final mass relation (Fig. 11.7a), are further evidence that AGB mass loss is very efficient at removing the stellar envelope.

The great majority of white dwarfs are indeed composed of C and O. Those with $M < 0.45\,M_\odot$ are usually He white dwarfs, formed by a low-mass star that lost its envelope already on the RGB. This is not expected to happen in single stars, but can result from binary interaction and indeed most low-mass WDs are found in binary systems. White dwarfs with $M > 1.2\,M_\odot$, on the other hand, are mostly ONe white dwarfs. They result from stars that underwent carbon burning in the core but developed degenerate ONe cores, which is expected to happen in a small initial mass range around $8\,M_\odot$.

The *surface* composition of white dwarfs is usually completely different than their interior composition. The strong surface gravity has resulted in separation of the elements, such that any hydrogen left is found as the surface layer while all heavier elements have settled at deeper layers. Most white dwarfs, regardless of their interior composition, therefore show spectra completely dominated by H lines and are classified as DA white dwarfs. A minority of white dwarfs show only helium lines and have spectroscopic classification DB. These have lost all hydrogen from the outer layers during their formation process, probably as a result of a late or very late thermal pulse.

11.2.1 Structure of white dwarfs

As discussed earlier, the equation of state of degenerate matter is independent of temperature, which means that the mechanical structure of a white dwarf is independent of its thermal properties. As a white dwarf cools, its radius therefore remains constant. As long as the electrons are non-relativistic the structure of a white dwarf can be described as a $n = \frac{3}{2}$ polytrope with constant K. Such stars follow a mass-radius relation of the form $R \propto M^{-1/3}$, depicted in Fig. 11.8 as a dashed line. A proper theory for WDs should take into account that the most energetic electrons in the Fermi sea can move with relativistic speeds, even in fairly low-mass white dwarfs. This means that the equation of state is generally not of polytropic form, but the relation $P(\rho)$ has a gradually changing exponent between $\frac{5}{3}$ and $\frac{4}{3}$, as shown in Fig. 3.3. The pressure in the central region is therefore somewhat smaller than that of a purely non-relativistic electron gas. Thus WD radii are smaller than given by the polytropic relation, the difference growing with increasing mass (and increasing central density). The relativistic theory, worked out by Chandrasekhar, predicts the mass-radius relation shown as a solid line in Fig. 11.8. As the mass approaches the Chandrasekhar mass, given by eq. (4.22),

$$M_{\rm Ch} = 1.459 \left(\frac{2}{\mu_{\rm e}}\right)^2 M_\odot, \tag{11.3}$$

the radius goes to zero as all electrons become extremely relativistic. White dwarfs more massive than $M_{\rm Ch}$ must collapse as the relativistic degeneracy pressure is insufficient to balance gravity.

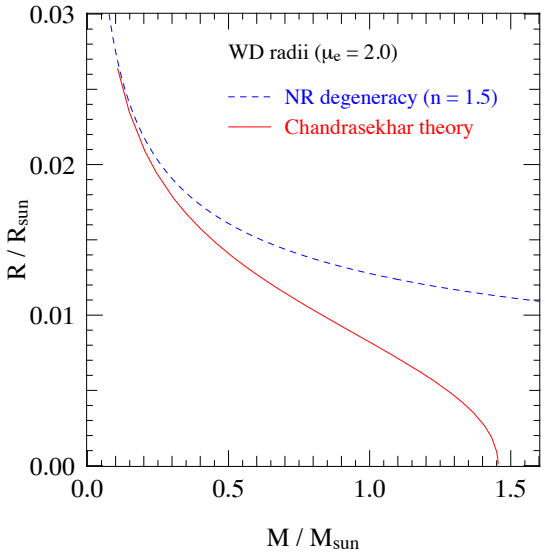

Figure 11.8. Comparison of the radius-mass relation of a completely degenerate star computed using Chandrasekhar's theory for white dwarfs (taking into account the partly relativistic velocities of the electrons in the Fermi sea) and an approximation based on non-relativistic degeneracy.

Chandrasekhar's white dwarf theory assumes the electrons are fully degenerate and non-interacting. In reality, certain corrections have to be made to the structure, in particular *electrostatic interactions* between the electrons and ions (see Sec. 3.6.1). These give a negative correction to the electron pressure, leading to a somewhat smaller radius at a particular mass. Furthermore, at high densities *inverse β-decays* become important. Examples are the reactions

$$^{24}\mathrm{Mg} + \mathrm{e}^- \rightarrow {}^{24}\mathrm{Na} + \nu, \qquad {}^{24}\mathrm{Na} + \mathrm{e}^- \rightarrow {}^{24}\mathrm{Ne} + \nu.$$

A neutron-rich nucleus such as ^{24}Na is normally unstable to β-decay ($^{24}\mathrm{Na} \rightarrow {}^{24}\mathrm{Mg} + \mathrm{e}^- + \bar{\nu}$), but at high density is stabilized by the Fermi sea of energetic electrons: the decay is prevented because the energy of the released electron is lower than the Fermi energy. Reactions such as these (also called *electron captures*) decrease the electron pressure at high density. Their main effect is a lowering of the effective Chandrasekhar mass, from the 'ideal' value of 1.459 $M_\odot$ for a CO white dwarf to 1.4 $M_\odot$.

11.2.2 Thermal properties and evolution of white dwarfs

In the interior of a white dwarf, the degenerate electrons provide a high thermal conductivity (Sec. 5.2.4). This leads to a very small temperature gradient, especially because L is also very low. The degenerate interior can thus be considered to a have a constant temperature. However, the outermost layers have much lower density and are non-degenerate, and here energy transport is provided by radiation. Due to the high opacity in these layers, radiation transport is much less effective than electron conduction in the interior. The non-degenerate outer layers thus act to insulate the interior from outer space, and here a substantial temperature gradient is present.

We can obtain a simple description by starting from the radiative envelope solutions discussed in Sec. 7.2.3, assuming an ideal gas and a Kramers opacity law $\kappa = \kappa_0 \rho T^{-7/2}$, and assuming P and T approach zero at the surface:

$$T^{17/2} = B\,P^2 \qquad \text{with} \qquad B = \frac{17}{4}\frac{3}{16\pi acG}\frac{\kappa_0\mu}{\mathcal{R}}\frac{L}{M}. \tag{11.4}$$

Replacing $P = (\mathcal{R}/\mu)\rho T$ and solving for ρ, we find that within the non-degenerate envelope

$$\rho = B^{-1/2}\frac{\mu}{\mathcal{R}}T^{13/4}. \tag{11.5}$$

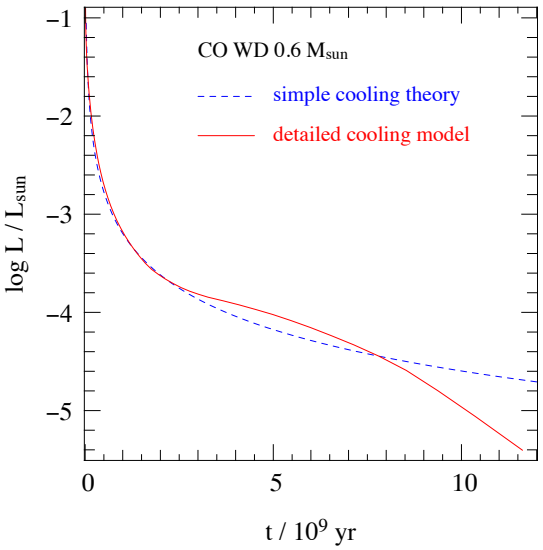

Figure 11.9. Theoretical cooling curves for a CO white dwarf with a typical mass of $0.6\,M_\odot$. The dashed (blue) line shows the evolution of luminosity with time based on the simple cooling theory by Mestel, which yields $L \propto t^{-7/5}$. The solid (red) line is a detailed cooling model for a DA white dwarf by M. Wood (1995, LNP 443, 41). This model takes into account (among other things) the effect of *crystallization*, a phase transition that releases an additional amount of energy, visible as the slowing down of the cooling after about 2 Gyr. When crystallization is almost complete after about 7 Gyr, the cooling speeds up again.

Let us assume that the transition point with the degenerate interior is located where the degenerate electron pressure equals the ideal-gas pressure of the *electrons* in the envelope, $P_\mathrm{e} = (\mathcal{R}/\mu_\mathrm{e})\rho T$, since the ions are non-degenerate everywhere. At this point, denoted with subscript 'b', we have

$$\frac{\mathcal{R}}{\mu_\mathrm{e}}\rho_\mathrm{b}T_\mathrm{b} = K_\mathrm{NR}\left(\frac{\rho_\mathrm{b}}{\mu_\mathrm{e}}\right)^{5/3}.$$

T_b and ρ_b must match the value given by eq. (11.5) at the transition point. Eliminating ρ_b gives

$$T_\mathrm{b}^{7/2} = \frac{\mathcal{R}^5\mu_\mathrm{e}^2}{K_\mathrm{NR}^3\mu^2}\,B = \frac{51\mathcal{R}^4}{64\pi acGK_\mathrm{NR}^3}\,\kappa_0\frac{\mu_\mathrm{e}^2}{\mu}\,\frac{L}{M}. \tag{11.6}$$

Since the degenerate interior is nearly isothermal, T_b is approximately the temperature of the entire interior or 'core' of the white dwarf. We can thus write (11.6) as $T_\mathrm{c}^{7/2} = \alpha\,L/M$. To evaluate the proportionality constant α we have to substitute appropriate values for κ_0 and the composition (μ_e and μ), which is somewhat arbitrary. Assuming bound-free absorption (eq. 5.33) and $\mu_\mathrm{e} = 2$ in the envelope, which is reasonable because the envelope is H-depleted except for the very surface layers, we get $\alpha \approx 1.38\times10^{29}\,Z/\mu$ in cgs units. In a typical DA white dwarf, most of the non-degenerate layers are helium-rich so assuming $Z = 0.02$ and $\mu \approx 1.34$ is reasonable. With these assumptions we obtain the following relation between the temperature in the interior and the luminosity and mass of the white dwarf,

$$T_\mathrm{c} \approx 7.7\times10^7\,\mathrm{K}\left(\frac{L/L_\odot}{M/M_\odot}\right)^{2/7}. \tag{11.7}$$

The typical masses and luminosities of white dwarfs, $M \approx 0.6\,M_\odot$ and $L < 10^{-2}\,L_\odot$, imply 'cold' interiors with $T < 2\times10^7$ K.

We can use these properties of white dwarfs to obtain a simple model for their cooling, i.e. the change in WD luminosity with time. Since there are no nuclear energy sources, the virial theorem applied to degenerate objects tells us that the luminosity radiated away comes from the decrease of internal energy. Since the electrons fill their lowest energy states up to the Fermi level, their internal energy cannot change and neither can energy be released by contraction. The only source of energy

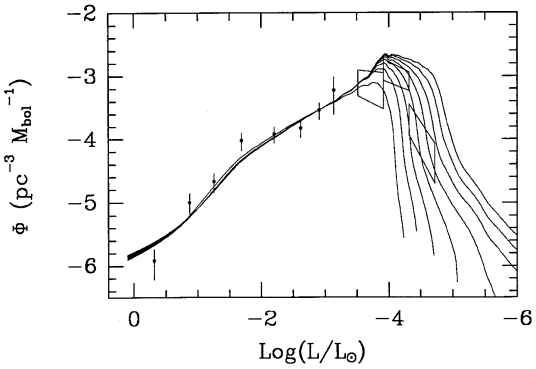

Figure 11.10. Observed and theoretical distributions of white dwarf luminosities in the Galactic disk, from Wood (1992, ApJ 386, 539), based on cooling models similar to the one shown in Fig. 11.9. The curves are for assumed ages of the Galactic disk between 6 and 13 Gyr. The paucity of observed white dwarfs with $\log(L/L_\odot) < -4.3$, shown as a slanted box, implies an age of the local Galactic disk of 8–11 Gyr.

available is the thermal energy stored in the non-degenerate ions, that make up the bulk of the mass of the white dwarf. Since the interior is isothermal at temperature T_c, the total thermal energy is

$$E_\mathrm{in} = c_V M T_\mathrm{c}, \tag{11.8}$$

where c_V is the specific heat per unit mass. For ions behaving as an ideal gas we have $c_V = \frac{3}{2}\mathcal{R}/\mu_\mathrm{ion}$ which is a constant. The luminosity is thus given by

$$L = -\frac{\mathrm{d}E_\mathrm{in}}{\mathrm{d}t} = -c_V M \frac{\mathrm{d}T_\mathrm{c}}{\mathrm{d}t}, \tag{11.9}$$

where L is related to M and T_c by eq. (11.6). If we write this relation as $T_\mathrm{c}^{7/2} = \alpha\, L/M$ we obtain

$$T_\mathrm{c}^{7/2} = -\alpha c_V \frac{\mathrm{d}T_\mathrm{c}}{\mathrm{d}t},$$

which can be easily integrated between an initial time t_0, when the white dwarf forms, and a generic time t to give

$$\tau \equiv t - t_0 = \frac{2}{5}\alpha c_V \,(T_\mathrm{c}^{-5/2} - T_{\mathrm{c},0}^{-5/2}). \tag{11.10}$$

Once the white dwarf has cooled significantly, its core temperature is much smaller than the initial value so that $T_{\mathrm{c},0}^{-5/2}$ can be neglected. We thus obtain a simple relation between the cooling time τ of a white dwarf and its core temperature, and thus between τ and the luminosity,

$$\tau \approx \frac{2}{5}\alpha c_V\, T_\mathrm{c}^{-5/2} = \frac{2}{5} c_V\, \alpha^{2/7} \left(\frac{L}{M}\right)^{-5/7}. \tag{11.11}$$

Making the same assumptions in calculating α as in eq. (11.7), and substituting $c_V = \frac{3}{2}\mathcal{R}/\mu_\mathrm{ion}$, we can write this relation as

$$\tau \approx \frac{1.05 \times 10^8\ \mathrm{yr}}{\mu_\mathrm{ion}} \left(\frac{L/L_\odot}{M/M_\odot}\right)^{-5/7}. \tag{11.12}$$

This approximate cooling law was derived by Mestel. It shows that more massive white dwarfs evolve more slowly, because more ionic thermal energy is stored in their interior. Also, increasing the mean mass of the ions μ_ion in a white dwarf of the same total mass decreases the cooling time, because there are fewer ions per unit mass storing heat. For a CO white dwarf composed in equal parts of C and O, $\mu_\mathrm{ion} \approx 14$.

This simple cooling law, depicted in Fig. 11.9 for a 0.6 $M_\odot$ CO white dwarf, predicts cooling times greater than 1 Gyr when $L < 10^{-3}\,L_\odot$, and greater than the age of the Universe when $L < 10^{-5}\,L_\odot$. More realistic models take into account the effect of contraction of the non-degenerate envelope, which provides some additional energy during the initial cooling phase, and more importantly, the effects of Coulomb interactions and of *crystallization* in particular. As the ion gas cools, electrostatic interactions become more important (Sec. 3.6.1) and the ions settle into a lattice structure. This releases latent heat (in other words, $c_V > \frac{3}{2}\mathcal{R}/\mu_{\rm ion}$) and the cooling is correspondingly slower than given by the Mestel law. Once crystallization is almost complete, c_V decreases and cooling speeds up again. A more detailed WD cooling model that includes these effects is shown in Fig. 11.9. White dwarfs that have cooled for most of the age of the Universe cannot have reached luminosities much less than $10^{-5}\,L_\odot$ and should still be detectable. Observed white dwarf luminosities thus provide a way to derive the age of a stellar population (e.g. see Fig. 11.10).

Suggestions for further reading

The evolution of AGB stars is treated in Chapter 26.6–26.8 of Maeder and Chapter 33.2–33.3 of Kippenhahn & Weigert. White dwarfs are discussed in more detail in Chapter 35 of Kippenhahn & Weigert and Chapter 7.4 of Salaris & Cassisi.

Exercises

11.1 Core mass luminosity relation for AGB stars

The luminosity of an AGB star is related to its core mass via the Paczynski relation (11.1). The nuclear burning in the H- and He-burning shells add matter to the core at a rate of $\dot{M}_c/M_\odot = 1.0\times10^{-11}(L_*/L_\odot)$. Assume that a star enters the AGB with a luminosity of $10^3\,L_\odot$ and a total mass of 2 $M_\odot$.

(a) Derive an expression for the luminosity as a function of time after the star entered the AGB phase.

(b) Assume that $T_{\rm eff}$ remains constant at 3000 and derive an expression for the radius as a function of time.

(c) Derive an expression for the core-mass as a function of time.

11.2 Mass loss of AGB stars

The masses of white dwarfs and the luminosity on the tip of the AGB are completely determined by mass loss during the AGB phase. The mass loss rate is very uncertain, but for this exercise assume that the mass loss rate is given by the Reimers relation, eq. (10.3), with $\eta \approx 3$ for AGB stars. Now, also assume that a star entered the AGB phase with a mass of 2 $M_\odot$ and a luminosity of $10^3\,L_\odot$.

(a) Derive an expression for the mass of the star as a function of time, using $L(t)$ and $R(t)$ from Exercise 11.1. (Hint: $-\dot{M}M = 0.5\,{\rm d}(M^2)/{\rm d}t$).

(b) Use the expression from (a) and the one for $M_c(t)$ from Exercise 11.1 to derive:

- the time when the star leaves the AGB ($M_{\rm env} \simeq 0$).
- the luminosity at the tip of the AGB.
- the mass of the resulting white dwarf. (This requires a numerical solution of a simple equation).

(c) Derive the same quantities in the cases when the mass loss rate on the AGB is three times larger, i.e., $\eta = 9$, and when it is three times smaller, i.e., $\eta = 1$.